Journal of Environmental Management 287 (2021) 112319

Contents lists available at ScienceDirect

Journal of Environmental Management

journal homepage: http://www.elsevier.com/locate/jenvman

Bipolar membrane reverse electrodialysis for the sustainable recovery of energy from pH gradients of industrial wastewater: Performance prediction by a validated process model

Andrea Culcasi, Luigi Gurreri *, Giorgio Micale, Alessandro Tamburini

Dipartimento di Ingegneria, Università Degli Studi di Palermo, Viale Delle Scienze Ed. 6, 90128, Palermo, Italy

ARTICLE INFO

Keywords:
pH gradient energy
Wastewater valorisation
Electro-membrane process
Ion-exchange membrane
Bipolar membrane reverse electrodialysis

ABSTRACT

The theoretical energy density extractable from acidic and alkaline solutions is higher than 20 kWh m^{-3} of single solution when mixing 1 M concentrated streams. Therefore, acidic and alkaline industrial wastewater have a huge potential for the recovery of energy. To this purpose, bipolar membrane reverse electrodialysis (BMRED) is an interesting, yet poorly studied technology for the conversion of the mixing entropy of solutions at different pH into electricity. Although it shows promising performance, only few works have been presented in the literature so far, and no comprehensive models have been developed yet. This work presents a mathematical multi-scale model based on a semi-empirical approach. The model was validated against experimental data and was applied over a variety of operating conditions, showing that it may represent an effective tool for the prediction of the BMRED performance. A sensitivity analysis was performed in two different scenarios, i.e. (i) a reference case and (ii) an improved case with high-performance membrane properties. A Net Power Density of ~15 W m^{-2} was predicted in the reference scenario with 1 M HCl and NaOH solutions, but it increased significantly by simulating high-performance membranes. A simulated scheme for an industrial application yielded an energy density of ~50 kWh m^{-3} (of acid solution) with an energy efficiency of ~80–90% in the improved scenario.

1. Introduction

1.1. BMRED process: state of the art and possible implementation for industrial wastewater

Many industrial sectors make extensive use of acidic and alkaline aqueous solutions at various concentrations, causing the disposal of high volumes of wastewater. For example, acid solutions are used in pickling processes for the hot-dip-galvanizing (Gueccia et al., 2020) or the electroplating industries (Agrawal and Sahu, 2009). In the case of the pickling process, the wastewater is typically neutralized utilizing an alkaline reagent (Goel et al., 2005). In this way, the pH gradient is entirely dissipated, thus losing the neutralization energy with both high economic costs (Culcasi et al., 2019) and environmental impact (Gueccia et al., 2020). In regard to basic solutions, large quantities come from ethylene plants (Imran et al., 2016), textile industries (Rahman and Khan, 2010), and the anodizing industry, which uses NaOH solutions for the removal of aluminium from extruder matrixes (Tansens et al., 2011). In order to reduce the treatment costs, a controlled neutralization of both acid and base wastes with a concurrent production of electric energy would be interesting.

Bipolar Membrane Reverse Electrodialysis (BMRED) is an innovative and sustainable technology that may accomplish this option. BMRED dates back to 1982 when Walther and Skaneateles (1982) published their patent. In its first conceptualization, this technology consisted of a single cell provided with an individual bipolar membrane (BPM) for the controlled neutralization of the acid and base solutions hosted in the two compartments. In fact, the bipolar membrane is able to drive the migration of proton and hydroxide ions through its respective selective layers (i.e. cation-exchange layer, CEL, and anion-exchange layer, AEL) (Pärnamäe et al., 2021). Analogously with the semi-conductors theory, the bipolar membrane during the BMRED process acts as a p-n junction under a forward bias (Ramírez et al., 1994). Subsequently, BMRED devices have been developed with several repetitive units stacked together, as in electrodialysis and bipolar membrane electrodialysis (BMED) units. Unlike BMED processes (Gurreri et al., 2020), BMRED has been studied so far in one configuration, i.e. the one with

* Corresponding author.
E-mail addresses: andrea.culcasi@unipa.it (A. Culcasi), luigi.gurreri@unipa.it (L. Gurreri), giorgiod.maria.micale@unipa.it (G. Micale), alessandro.tamburini@unipa.it (A. Tamburini).

https://doi.org/10.1016/j.jenvman.2021.112319
Received 5 December 2020; Received in revised form 16 January 2021; Accepted 1 March 2021
Available online 13 March 2021

Nomenclature

Symbols

a	(mol m^{-3}) ion activity
b	(m) spacer width
C	(mol m^{-3}) molar concentration
D	(m^2 s^{-1}) diffusion coefficient
E	(V) triplet electromotive force corrected for concentration polarization
EMF	(V) triplet electromotive force
F	(C mol^{-1}) Faraday constant
G	(kg m^{-2} s^{-1}) mass flux
GED_m	(kWh kg^3) gross energy density per kg of HCl
GED_m	(kWh m^3) gross energy density per m^3 of HCl
GPD	(W m^{-2}) gross power density
i_c	(A m^{-2}) current density
I	(A) current intensity
J	(mol m^{-2} s^{-1}) effective molar flux
J^*	(mol m^{-2} s^{-1}) apparent molar flux
L	(m) spacer length
M	(g mol^{-1}) molar mass
n	(−) number of ion species
N	(−) number of triplets
NPD	(W m^{-2}) net power density
PPD	(W m^{-2}) pumping power density
Q	(m^3 s^{-1}) volume flow rate
R	(Ω) generic electric resistance
R_g	(J mol^{-1} k^{-1}) gas constant
t_i	(−) effective ion transport number
t_i^*	(−) apparent ion transport number
T	(K) temperature
U	potential difference over the series of resistances R_u and R_{bl}
U_{ext}	potential difference over the external load R_u
ΔV	(V) generic voltage difference
X	(mol m^{-3}) fixed charge density in the membrane
z	(−) ion charge

Greek letters

δ	(−) Kronecker delta
η_c	(−) current efficiency
τ	(−) HCl consumption

Subscripts/superscripts

a	acid
ac	acidic solution/bipolar membrane interlayer interface
av	average over the triplet
AEL	anionic exchange layer
ba	alkaline solution/bipolar membrane interlayer interface
bl	blank
bp	interlayer of the bipolar membrane
BPL	bipolar membrane layer
co	co-ion
ct	counter-ion
CEL	cationic exchange layer
$diff$	diffusive
ext	external
i	ion species
in	inlet
int	interface
j	ion species
k	generic cell-triplet in the stack
out	outlet
s	salt
$salt$	salt
sol	solution
th	theoretical
u	external load

Acronyms/abbreviations

AEL	Anion-Exchange Layer
AEM	Anion-Exchange Membrane
BMED	Bipolar Membrane ElectroDialysis
BMRED	Bipolar Membrane Reverse ElectroDialysis
BPM	Bipolar Membrane
CEL	Cation-Exchange Layer
CEM	Cation-Exchange Membrane
ED	ElectroDialysis
GPD	Gross Power Density
IEM	Ion Exchange Membrane
OCV	Open Circuit Voltage
RED	Reverse ElectroDialysis

three-compartment repeating units, i.e. acid, base and salt, with three membrane types, i.e. cation-exchange membrane (CEM), anion-exchange membrane (AEM) and BPM (Fig. 1).

BMRED is exactly the opposite process of BMED, converting chemical energy, in the form of a pH gradient, into electricity for final users. This occurs by neutralization at the interlayer of the BPM. The neutralization reaction is a very energetic process that, on the one hand, causes the production of water molecules from proton and hydroxide ions, and, on the other hand determines the passage of the respective conjugated base (Cl^- ions) and acid (Na^+ ions) from the acid and base channels to the salt compartment. In this way, the electroneutrality is satisfied. The ion current is then converted into electricity in the external circuit thanks to the redox reactions at the electrode compartments. The neutralization reaction involves a Gibbs energy at 25 °C and 1 bar equal to −80 kJ mol^{-1}, which corresponds to an energy density of ~22 kWh m^{-3} of acidic (or basic) solution at a concentration of 1 M (0.83 V of electromotive force (Xia et al., 2018)) and to an energy density of ~100 kWh m^{-3} at a concentration of 5 M. However, the high selectivity of current membranes is compatible with maximum concentrations of ~1–2 M. In order to implement techno-economic competitive BMRED processes, further studies should develop high-performance membranes able to limit co-ion leakages under severe operating conditions in terms of acid and base concentration, as well as over long-run operations. For instance, bipolar membranes should have very high selectivity to proton and hydroxide ions in CEL and AEL, respectively, as well as high water permeability. The latter is a very important characteristic as the amount of water molecules produced by the acid-base neutralization is very high at high current densities. Therefore, the water permeability of the BPM is crucial to avoid any risk of delamination, even at high current densities (Xia et al., 2018).

Moreover, BMRED deals with highly conductive solutions that may give rise to quite a few problems in terms of parasitic currents, i.e. the ionic current by-pass through the manifolds instead of across the membranes (Culcasi et al., 2020a). Another detrimental phenomenon is the power consumption due to the pumping of the solutions. This is crucial for reverse electrodialysis systems, because the higher the pumping power, the lower the available power for the final user. In this respect, BMRED takes advantage of a high energy density, which is (at a concentration of 1 M of acid and base) ≈ 1 order of magnitude higher than the energy released by mixing salt and fresh water.

Despite BMRED represents an interesting technology for converting pH gradients into electricity, it has been poorly investigated. The very

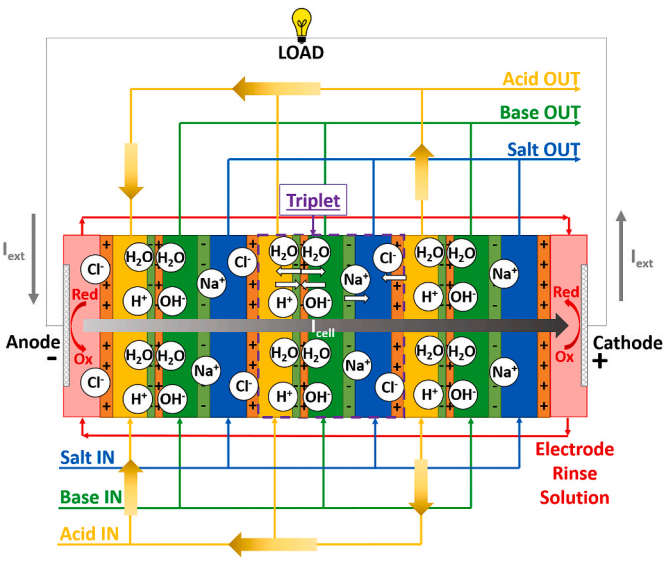

Fig. 1. Scheme of a Bipolar Membrane Reverse Electrodialysis (BMRED) stack. The large grey arrow from the anode to the cathode indicates the desired direction of the electric current; the large yellow arrows indicate the parasitic electrical pathways (shortcuts) via manifolds in the hydraulic circuit of the acid solution. (For interpretation of the references to colour in this figure legend, the reader is referred to the Web version of this article.)

few works presented in the literature regard BMRED as the discharge phase of the Acid-Base Flow Battery (Pärnamäe et al., 2020).

Emrén and Holmström (1983) explored the battery using a seven-triplet stack, recording a maximum output voltage of 1.8 V (current density of ~1.4 A m^{-2}) with an estimated permselectivity of the BPMs of ~50% during the discharge experiment.

Pretz and Staude (1998) studied the range of concentration of 0.1–1 M of acid and base. The current efficiency decreased by one order of magnitude when passing from 0.1 to 1 M due to the non-ideal behaviour of the IEMs. By changing the BPM type, the maximum energy efficiency of the process was 22%. In terms of voltage-current trend, by using an external resistance equal to the internal one, the stack voltage is theoretically 50% of the open circuit voltage. However, a lower electric potential was observed, and this was attributed to the higher electric resistance (up to 15 times increase) due to water accumulation in the bipolar membrane interlayer at higher electric currents. The water flux may also irreversibly damage the BPMs through delamination.

Zholkovskij et al. (1998) investigated a 4-compartment BMRED stack. The measured values of membrane resistance were 5, 2 and 6.8 Ω cm^2 for AEM, CEM and BPM, respectively. They explored very low values of current densities (up to ~2 A m^{-2}) and low-concentration solutions (~0.03 M). They reported a specific energy of 0.1 Wh kg^{-1} and a maximum power density of 0.005 W kg^{-1}.

Kim et al. (2016) explored the acid/base concentration range of 0.1–0.7 M with a single-cell stack, obtaining a maximum GPD of 2.9 W m^{-2} of total membrane area. The open circuit voltage (OCV) was 6% lower on average than the theoretical one. This discrepancy was explained by two reasons: i) the effect of the excessive water formation due to the neutralization reaction in the interlayer and ii) the overvoltage of the electrode reactions. Particularly, the greater reductions in electric potential were found to occur at higher concentrations, where the water formation in the interlayer was higher.

Van Egmond et al. (2018) performed experiments by using a single-triplet stack with active membrane area of 0.01 m^2 and 0–1 M HCl and NaOH solutions. The OCV was found to be 0.83 V at 1 M of acid and base, corresponding to 89% of apparent permselectivity of the membrane stack. Moreover, they performed discharge tests with current densities in the interval 5–15 A m^{-2}. The delamination of the BPM was observed at 20 A m^{-2}. A maximum GPD of 3.7 W m^{-2} and a specific energy density of 2.9 Wh kg^{-1} were achieved.

Xia et al. (2018) first investigated BMRED units with a single triplet. Then, the same authors used a variable number of repetitive units in the range of 5–20 (Xia et al., 2020). The single triplet experiments were performed with acid and base concentration in the range of 0–1 M (Xia et al., 2018). Stack experiments (Xia et al., 2020) were performed with acid/base concentration equal to 1 M or 0.5 M. Single cell experiments showed that the maximum achievable specific power was ~95 W kg^{-3} (Xia et al., 2018). Compared to the other works presented in literature, this value seems to be unrealistic, as it should correspond to a GPD of ~60 W m^{-2}. The OCV values measured by varying the number of repeating units (from 5 to 20) were lower than the values calculated by a linear extrapolation of the OCV for a single triplet [49]. Particularly, the higher the number of triplets, the higher the discrepancy. This was due to the detrimental effects of the shunt currents through the manifolds. However, a maximum GPD of ~17 W m^{-2} (excluding electrode losses) was found with a stack equipped with 20 triplets, at a current density of 100 A m^{-2} (Xia et al., 2020). Moreover, delamination issues did not occur up to 200–400 A m^{-2} (Xia et al., 2020).

In a previous work of our research group, lab-scale BMRED experiments were performed, obtaining a maximum GPD of 17 W m^{-2} at 100 A m^{-2} with a 10-triplet stack fed with single pass by 1 M HCl and NaOH solutions (Zaffora et al., 2020). From experiments at different inlet concentration, an energy density of ~10 kWh m^{-3} acid was estimated for a complete neutralization. Parasitic currents were significant when the stack was equipped with a higher number of triplets. At 1 M acid and base, the apparent permselectivity was of 93% for a five-triplet stack, while it decreased to 54% for a 38-triplet stack, which delivered a ~35% lower GPD. The presence of NaCl in the acidic and alkaline solutions had important effects only with a high number of triplets, by reducing the GPD by 23.4–45.7%.

1.2. BMRED modelling: state of the art

Conventional RED processes have been studied by a wide variety of mathematical models, including several simulation approaches from simplified lumped parameters models to more complex multi-physics and multi-scale models. The simplified models allow the prediction of the RED behaviour only qualitatively as they are based on numerous simplifying assumptions. On the other hand, the advanced ones try to simulate with high accuracy the process at a cost of a large computational burden. Some numerical models have been based on the Nernst-Planck theory (Generous et al., 2020; Tedesco et al., 2017) or on the more rigorous Stefan-Maxwell approach (Kraaijeveld et al., 1995). However, the most effective method is based on a separation of spatial scales and the use of accessible empirical parameters characterizing the membrane properties. These multi-scale semi-empirical models describe the ED/RED process behaviour by solving material mass balances for the repetitive units calculating membrane fluxes and requiring, as only input, membrane characteristics. They have been developed for ED and/or RED (La Cerva et al., 2019), allowing for the study of several aspects and configurations including, for example, the use of capacitive electrodes (Campione et al., 2020), parasitic currents via manifolds (Culcasi et al., 2020a) and cross-flow stacks with or without deformation effects (Battaglia et al., 2021). The main feature of this class of models is that they represent a good compromise in terms of predictive accuracy and computational cost. Therefore, they can serve for large simulation campaigns, including optimisation studies (Ciofalo et al., 2019).

Unlike the conventional RED, very few modelling attempts have been presented so far in literature for the BMRED process. The set of equations reported by Pretz and Staude (1998) represents a simplified lumped model, in which the OCV was calculated as proportional to the cells number. Moreover, the evaluation of the gross power and the internal resistance were proposed. The model predictions were not in a good agreement with the experimental data, especially the OCV, for

which an important discrepancy was observed by increasing the number of repetitive units, due to the occurrence of parasitic currents.

Zholkovskij et al. (1998) elaborated a 1-D model, in which variables are not discretized along the direction of flow but rather along the direction of the membrane fluxes. In this model, the EMF is calculated by considering not only the bipolar membrane electrical potential but also the one related to the homopolar membranes. Furthermore, parameters as specific capacity, energy density and power density were assessed. To obtain these system characteristics, the calculation of the external voltage by varying the current portion for a fixed discharge time was proposed. The developed equations were simplified by considering two limiting conditions, i.e. very slow or rapid process. They obtained a complex system of equations which presents quite a few resolution difficulties as well as the need of not easily empirically accessible parameters. Despite the numerical complexity, the maximum discrepancy with the experimental results was high, in the order of 30%. Therefore, this model aimed at predicting only qualitative trends of the BMRED process.

Xia et al. (2018) did not develop a predictive model, but they only calculated some performance indicators, as the stack voltage, power density and the voltage efficiency by using the experimental OCV, the external current and the internal resistance. The expression used for the theoretical OCV was derived from the ion electrochemical potential equations at the membrane-solution interfaces.

Despite its great potential, the BMRED process has been poorly studied so far. This work presents the first comprehensive mathematical modelling tool of BMRED systems. A semi-empirical multi-scale model was developed in order to predict the behaviour of the BMRED process and the main figure of merits of relevant interest. Once experimentally validated, the model was used to perform a sensitivity analysis to give insights about the potential of this innovative technology for energy harvesting by neutralization of acidic and alkaline industrial wastewater.

2. Description of the multi-scale model

The present mathematical model was developed in the gPROMS Model Builder® platform with a multi-scale structure. The model presents four levels and three dimensional scales. Except for the bipolar membrane level, where more significant changes were required, the equations adopted at the various levels or dimensional scales are the same or with only small changes with respect to those reported in our previous work (Culcasi et al., 2020b). Table 1 reports the modelled scales and the relative levels.

In the following sections, the modifications regarding the bipolar membrane level and other model levels, when needed, will be described. Finally, the main performance parameters relevant for the BMRED technology will be defined, e.g. energy density and efficiency.

2.1. Low scale: channel model

This model was described in a previous work (Culcasi et al., 2020b). The model integrates correlations coming from Computational Fluid Dynamic (CFD) simulations for the calculation of Sherwood numbers and friction factors along the channels and pressure drops at the inlet/outlet regions of the channels connected to the manifolds. All the equations and considerations are still valid without any modifications.

Table 1
Summary of the modelled scales and levels.

Model scale	Model level	Reference
Low	Channel	Culcasi et al. (2020b)
	Bipolar membrane	Present work
Middle	Triplet	Culcasi et al. (2020b)
High	Stack	Culcasi et al. (2020b)

2.1.1. Low scale: bipolar membrane model

The bipolar membrane is modelled with two layers, i.e. CEL and AEL, and an interlayer in which no mass accumulation is assumed. All the bipolar membranes of a stack are simulated and discretized along the flow direction. Likewise the case of homopolar membranes, bipolar membrane fluxes are evaluated by adopting the Nernst-Planck-Donnan approach for multi-ion systems (Kontturi et al., 2008). The multi-ion system is simulated with four ions: Na^+, H^+, Cl^-, OH^-. The ion transport through the bipolar membrane layers is given by:

$$J_{i,BPL} = -J_{diff,i,BPL} + \frac{t_{i,BPL}\, i_c}{z_i\, F} \tag{1}$$

in which $J_{i,BPL}$ is the total molar flux of the i-th ion across the generic bipolar membrane layer (i.e. CEL or AEL), $J_{diff,i,BPL}$ is the diffusive component of the ion flux, $t_{i,BPL}$ is the transport number of the i-th ion within the layer, i_c is the current density, z_i is the ion charge and F is the Faraday constant. $J_{i,BPL}$ is positive if entering the channel, negative if exiting the channel.

However, the ion fluxes through the bipolar membrane layers have to satisfy the overall electroneutrality over the BPM. In order to satisfy both the electroneutrality condition and the assumption of no accumulation in the BPM-interlayer, diffusive and migrative fluxes (the first and the second addend in Eq. (1)) must be properly evaluated. For this reason, the migrative flux in each bipolar membrane layer is computed with "effective" ion transport numbers $t_{i,BPL}$, which are calculated as the half-sum of the "apparent" transport numbers $t^*_{i,BPL}$ of the correspondent counter- and co-ions in the two layers. In formulae:

$$t_{Cl,\,AEL} = t_{Na,\,CEL} = \frac{t^*_{Cl,AEL} + t^*_{Na,CEL}}{2} \tag{2}$$

$$t_{Na,\,AEL} = t_{Cl,\,CEL} = \frac{t^*_{Na,AEL} + t^*_{Cl,CEL}}{2} \tag{3}$$

$$t_{OH,\,AEL} = t_{H,\,CEL} = \frac{t^*_{OH,AEL} + t^*_{H,CEL}}{2} \tag{4}$$

$$t_{H,\,AEL} = t_{OH,\,CEL} = \frac{t^*_{H,AEL} + t^*_{OH,CEL}}{2} \tag{5}$$

Taken individually, the apparent ion transport numbers $t^*_{i,BPL}$ for each layer are related to the ion diffusion coefficients of all the ions and to the average ion concentration within the layer by the expression:

$$t^*_{i,BPL} = \frac{z_i^2 D_{i,BPL} \overline{C_{i,BPL}}}{\sum_j z_j^2 D_{j,BPL} \overline{C_{j,BPL}}} \tag{6}$$

in which $D_{i,BPL}$ is the diffusion coefficient of the i-th ion, and $\overline{C_{i,BPL}}$ is the average ion concentration within the bipolar membrane layer. $D_{i,BPL}$ is a tuning parameter of the model.

The following n-1 Donnan equilibrium equations at each membrane-solution interface are applied

$$\frac{R_g T}{z_i F} \ln \frac{C_{i,sol,int}}{C_{i,BPL,int}} = \frac{R_g T}{z_{i+1} F} \ln \frac{C_{i+1,sol,int}}{C_{i+1,BPL,int}} \tag{7}$$

where $C_{i,sol,int}$ and $C_{i,BPL,int}$ are the ion concentrations at the interface in the solution and membrane side, respectively, R_g is the gas constant and T is the temperature.

The electro-neutrality within each bipolar membrane layer is considered with the general expression:

$$X + \sum C_{co,BPL} = \sum C_{ct,BPL} \tag{8}$$

where X is the fixed charge group concentration in the IEM, $C_{co,BPL}$ and $C_{ct,BPL}$ are the co-ion and counter-ion concentrations in the bipolar membrane layer.

The effective diffusive fluxes $J_{diff,i,BPL}$ in each bipolar membrane layer have to satisfy the overall electroneutrality. For this reason, the effective ion diffusive flux is calculated as the half-sum of the apparent ion flux of the correspondent counter-ions (i.e., Na^+ and H^+ in CEL, and Cl^- and OH^- in AEL) and co-ions (i.e., Na^+ and H^+ in AEL, and Cl^- and OH^- in CEL) in the two layers (Eq. (9)). Particularly, the correspondent co-ions in CEL are Cl^- and OH^- for Na^+ and H^+ respectively and vice-versa for AEL.

$$J_{diff,i,CEL} = \frac{J^*_{diff,i,CEL} + J^*_{diff,i,AEL}}{2} \tag{9}$$

$$J_{diff,i,AEL} = -J_{diff,i,CEL} \tag{10}$$

According to the diffusion-conduction (Kontturi et al., 2008), the apparent diffusive flux of the ion species i through any layer of a BPM is

$$J^*_{diff,i,BPL} = -\sum_j D_{i,j,BPL} \nabla C_{j,BPL} \tag{11}$$

where $C_{j,BPL}$ is the concentration in the membrane phase of the j-th ion, $j = 1, 2, \ldots, n$ (where n is the number of ion species, which is 4 in the present work) in one or the other BPM layer. $J^*_{diff,i,BPL}$ is positive when the ion species exits the channel.

The concentration gradients are calculated by assuming a linear profile between the boundary values of concentration calculated by solving the Donnan equilibrium expressions (Eq. (7)). $D_{i,j,BPL}$ is the cross-diffusion coefficient, expressed as follows:

$$D_{i,j,BPL} \equiv D_{i,BPL}\delta_{ij} + \frac{t^*_{i,BPL}}{z_i} z_j \left(D_{i,BPL} - D_{j,BPL}\right) \tag{12}$$

where δ_{ij} is the Kronecker delta.

Particularly, since $J^*_{diff,i,BPL}$ is positive when the ion species exits the channel, the following relation is applied:

$$J_{diff,i,CEL} = -J_{diff,i,AEL} \tag{13}$$

The concentration gradient $\nabla C_{j,BPL}$ in Eq. (11) can be calculated by knowing the ion concentration at the interlayer interfaces, membrane side.

In the BPM interlayer $C_{j,BPL}$ is assumed to be null for the co-ions in their respective BPM-layer. However, for the counter-ions across the CEL, the Na^+ concentration is assumed to be constant and the H^+ concentration follows from the electro-neutrality relation; for the counter-ions across the AEL, the Cl^- concentration is assumed to be constant and OH^- concentration follows the electro-neutrality relation.

Finally, by following the assumption of no mass accumulation in the interlayer, a further salt flux should be considered to satisfy mass balances through the bipolar membrane system. Particularly, this salt mass flux (G_{salt}) is due to the migration of sodium and chloride ions through the bipolar membrane layers. It is computed as follows:

$$G_{salt,BPL} = -\frac{\left(t_{Na,BPL} + t_{Cl,BPL}\right) i_c}{2F} M_{NaCl} \cdot 10^{-3} \tag{14}$$

where M_{NaCl} is the molar mass of the sodium chloride.

2.2. Middle-low scale: triplet model

The equations have already been presented in a previous work (Culcasi et al., 2020b).

2.3. Middle-high scale: stack model

In the BMRED process, the produced electricity is conveyed along the external electric circuit toward an external load, which represents the final user. For the BMRED process, the equivalent electric circuit solved by the electrical sub-model of stack is shown in Fig. 2.

The cell current I_k for the k-th node and the external current I_{ext} are calculated as:

$$I_k = \frac{\left(E_{av,k} - \Delta V_k\right)}{R_{av,k}} \tag{15}$$

$$I_{ext} = \frac{U}{R_u + R_{bl}} \tag{16}$$

where $E_{av,k}$ is the average voltage generated by the cell triplet, ΔV_k is the k-th voltage difference over the cell triplet electric resistances; R_u, R_{bl} and $R_{av,k}$ are the external, the blank and the average cell resistance of the k-th cell; U is the potential difference over the series of R_u and R_{bl} resistances.

The gross power density GPD per total membrane area provided to the external load, can be simply calculated as

$$GPD = \frac{I_{ext}\, U_{ext}}{3\, N\, b\, L} \tag{17}$$

where $b{\cdot}L$ is the active area of one single membrane and U_{ext} is the potential difference over the external resistance R_u.

The net power density (NPD) is calculated as

$$NPD = GPD - PPD \tag{18}$$

where PPD is the pumping power density, calculated by the hydraulic model.

PPD can be calculated as

$$PPD = \frac{\Delta P_{tot,a} Q_{in,a} + \Delta P_{tot,b} Q_{in,b} + \Delta P_{tot,s} Q_{in,s}}{\chi\, 3N\, b\, L} \tag{19}$$

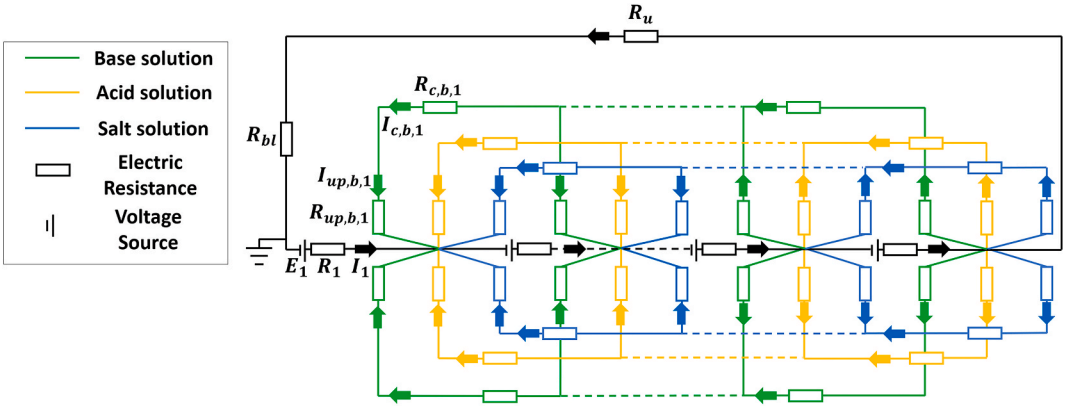

Fig. 2. Scheme of the equivalent electric circuit of BMRED stacks.

where $\Delta P_{tot,sol}$ and $Q_{in,sol}$ are the total pressure drop in the stack and the total volume flow rate at the stack inlet, respectively, for the generic solution *sol* (i.e., acidic, basic or salt solution).

2.4. Figures of merit of BMRED processes

In this section, the main figures of merit characterizing BMRED units are defined for steady state single pass operations. The mass Gross Energy Density (GED_m) represents the energy recovered by the process neutralizing 1 kg of HCl. It is given by

$$GED_m = \frac{U_{ext}\, I_{ext}}{3,600\, M_{HCl}\, Q_{in,a}\, \left(C_{H,a,in} - C_{H,a,out}\right)} \tag{20}$$

where GED_m is expressed in kWh kg_{HCl}^{-1}, M_{HCl} is the molar mass of the hydrochloric acid, and $C_{H,a,in}$ and $C_{H,a,out}$ are the proton concentrations in the acid solution at the stack inlet and outlet, respectively.

The current efficiency (η_c) was calculated as the ratio of the amount of protons migrating towards the interlayer of the BPMs over the actual amount of protons removed from the acid compartments (mass balances). It is calculated as

$$\eta_c = \frac{I_{ext} \sum_k t_{H,\ CEL,k}}{F\, \left(Q_{in,a}\, C_{H,a,in} - Q_{out,a}\, C_{H,a,out}\right)} \tag{21}$$

in which $Q_{out,a}$ is the total volume flow rate of the acid solution at the stack outlet.

The relative consumption of the hydrochloric acid in the acid compartments is calculated as:

$$\tau = \frac{Q_{in,a}\, C_{H,a,in} - Q_{out,a}\, C_{H,a,out}}{Q_{in,a}\, C_{H,a,in}} \tag{22}$$

Another important performance parameter is the energy density per unit volume of processed solution. The gross energy density (i.e., neglecting the energy loss due to pumping) is calculated as:

$$GED_v = \frac{U_{ext}\, I_{ext}}{3.6{\cdot}10^6 {\cdot} Q_{in,a}} \tag{23}$$

Moreover, the energy efficiency of the process is evaluated as:

$$\eta_{BMRED} = \frac{GED_v}{GED_{v,th}} \tag{24}$$

in which $GED_{v,th}$ is the theoretical gross energy density (kWh m^{-3}) calculated as follows:

$$GED_{v,th} = \frac{F}{3.6{\cdot}10^6} \int_{10^{-4}}^{C_{HCl,a,in}} EMF\ dC_{HCl,a,in} \tag{25}$$

where *EMF* is the electromotive force (V), which is calculated following the Nernst equation (Tanaka, 2007).

3. Experimental

BMRED experiments were collected by using a commercial lab-scale module (FT-ED-100) purchased from Fumatech BWT GmbH (Germany). The stack was equipped with the following IEMs: fumasep® FAB, fumasep® FKB and fumasep® FBM as AEM, CEM and BPM, respectively. DSA (Dimensionally Stable Anode)-type electrodes with an area of 10 × 10 cm^2 were used. IEMs were separated by PVC/ECTFE spacers (made by woven filaments and with a thickness of 500 μm). Spacers had three inlet/outlet of 8.5 mm diameter. The membrane active area was 10 × 10 cm^2. The stack was assembled with different number of repeating units in the interval 5–38. Acid, base and salt solutions were prepared using Hydrochloric Acid (HCl 37% Merck), Sodium Hydroxide (NaOH 98–100% Honeywell Fluka) and Sodium Chloride (NaCl 99.7% ChemSolute), respectively. The electrode rinse solution was an aqueous solution 0.5 M in $FeCl_2/FeCl_3$ (99% ChemSolute) and 0.6 M in HCl, added to prevent possible iron oxy-hydroxide precipitation (Veerman et al., 2010). Feeding solutions were prepared by using demineralized water. The experiments were performed with three different acid and base concentrations, i.e., 0.2, 0.6 and 1 M, as well as with or without the presence of 0.25 M NaCl of salt background in the acid and base compartments. The NaCl concentration at the inlet of the salt channels was kept constant at 0.25 M for all the experiments. The tests were performed by varying the number of triplets from 5 to 38 for the set of experiments without the presence of salt background, and from 5 to 30 for the set of experiments with the presence of salt background.

The AEM was used as end-membrane. Peristaltic pumps (BT601S, Lead Fluid Technology, CO LTD, China) were used for circulating all the acid, base and salt streams as well as the electrode rinse solution. A BK Precision 8540 DC Electronic Load, allowing the operation with galvanostatic mode, was used in the external circuit. All the experiments were re-tested a minimum of two times to verify their reliability. Inlet and outlet solution samples were collected for the analysis of both titration and chromatography to compare the ion concentrations in each compartment. Ion chromatography was performed with the Ion Chromatography (IC) Metrohm 882 Compact IC plus. Milli-Q water was used to prepare each sample to be used for chromatography.

A once-through (i.e., single pass) operation mode was used for all the experiments, i.e., the solutions from the inlet tanks flowed through the stack and were collected in the outlet tanks (Fig. 3). Once the pumps started flowing the electrolyte solutions through the stack, they operated for at least 5 min to ensure good membrane conditioning. Subsequently, the external circuit was closed by setting the load to provide the desired electric current. The operation continued until reaching a constant external voltage, and then samples of the outlet solutions were collected to determine pH and ion concentrations.

All experimental data were collected for model calibration and validation and some of them are also reported in our previous work (Zaffora et al., 2020), where the same experimental apparatus and methodology is employed. The latter are described above for the sake of completeness and clarity.

4. Results and discussion

4.1. Model validation at laboratory scale

The experiments were conducted with current density within the range from 0 to 29 A m^{-2}, to avoid the delamination of the BPMs. The model was calibrated by varying the ion diffusivities in the membranes. The values reported in Table 2 were used.

The electrical resistances of the monopolar membranes used in this

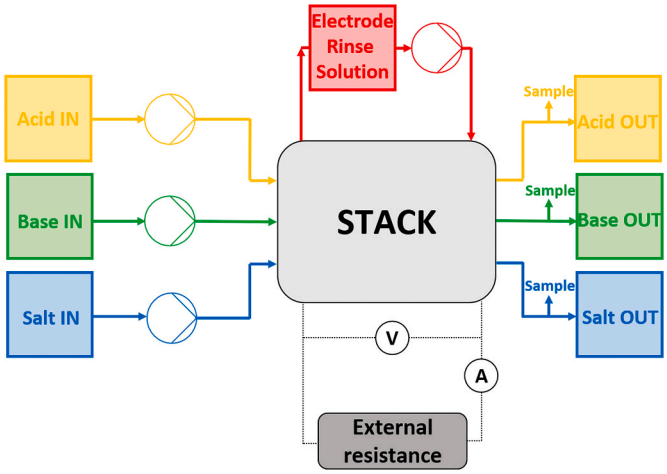

Fig. 3. Scheme of the adopted experimental set-up.

Table 2
Membrane properties used in the simulations.

Fixed properties					
		AEM	CEM	AEL	CEL
Thickness	μm	130	130	95	95
Water permeability	ml bar^{-1} h^{-1} m^{-2}	8	8	–	–
Areal resistance[a]	Ω cm^2	7	6	6.5	6.5
Fixed charge density	mol m^{-3} H_2O	5000	5000	5000	5000
Properties tuned for model calibration					
		AEM	CEM	AEL	CEL
H^+ diffusivity	m^2 s^{-1}	1.4E-10	4.7E-11	2.0E-11	3.4E-11
Na^+ diffusivity	m^2 s^{-1}	4.7E-11	1.6E-11	1.6E-11	0.5E-11
Cl^- diffusivity	m^2 s^{-1}	8.5E-11	2.8E-11	1.7E-11	0.6E-11
OH^- diffusivity	m^2 s^{-1}	0.9E-10	3.1E-11	0.9E-10	0.6E-11

[a] In the presence of background salt, the areal resistances observed experimentally were ~35% higher. This behaviour was taken into account in the model.

work are provided by the manufacturer, while that of the bipolar membrane is not provided (Fumatech BWT GmbH, 2021). Therefore, the electrical resistance of the bipolar membrane was estimated as a series of the three resistances of CEL, AEL and interlayer (Strathmann et al., 1997). The fixed charge density (FCD) was calculated as the ratio of the Ion-Exchange Capacity (IEC) and the swelling degree (SD), multiplied by the water density. The IEC is provided by the manufacturer for the AEM and the CEM (Fumatech BWT GmbH, 2021), but it is not available for the BPM. The SD is not provided for any of the three membranes. Unfortunately, these data are also lacking in the literature. However, the SD values of Fumasep FKD and FKS membranes have been reported (Mei and Tang, 2018), and were used to calculate the FCD. Finally, the value of water permeability reported in Table 2 is for membranes used in conventional electrodialysis (La Cerva et al., 2018), since the specific water permeability for the membranes used in this work was not found in the literature.

The polarization curves from experiments conducted without the presence of salt background (Fig. 4a, c and e) showed high repeatability since the average empirical error was ≈2.3%. Overall, the model predictions were in good agreement with the experimental data, regardless of the number of triplets as well as the inlet acid/base concentration. The overall average discrepancy was ≈2.4%, with a maximum discrepancy obtained for the 10-triplet stack with an inlet acid/base of 0.6 M, which was characterized by an average discrepancy of 6.5%.

The results illustrated in Fig. 4b, d and e concern the set of experiments conducted with the presence of background salt in the acid and base compartments. The experimental data again demonstrate high repeatability since the reported average deviation with the test-retest process was ≈2.9%. The model simulations were in good agreement even when varying the number of triplets. Particularly, the overall average variation was ≈3.3%. The maximum discrepancy was recorded for the experiments performed at 5 triplets with an inlet acid/base of 0.2 M, where an average relative error of ~7.4% was found.

Overall, the above results show the validity of the developed model for the prediction of the polarization curves of BMRED systems at different number of repetitive units, across a wide range of acid and base concentrations (i.e., 0.2–1 M), and with or without the effect of the background salt in the acid and base compartments.

The comparison between model predictions and experimental data was also made in terms of the outlet ion-concentrations. The tests were performed by using a variable number of triplets (38, 30, or 20), at a fixed mean channel flow velocity of 1 cm s^{-1}, and without the presence of NaCl as salt background in the acid and base channels. A fixed current density equal to 29 A m^{-2} was used for all the experiments. The inlet composition and concentrations are reported in Table 3. Titration and chromatography were repeated at least once, finding negligible errors.

Model outcome and experimental results are compared in Fig. 5.

Fig. 5 suggests that, apart from a few isolated cases, the outlet ion concentrations were predicted with good agreement with the experimental data. The average error in absolute terms was 3.2%, being 2.0%, 2.6% and 5.0% for the acid, base and salt solutions, respectively.

4.2. Industrial-scale stack simulations

In this section, the BMRED potential was investigated by considering the neutralization of hydrochloric acid and sodium hydroxide solutions. The presence of backgraund salt in the acidic and alkaline solution was simulated, mimicking the use of waste streams. The simulations were performed with stacks provided with 50 triplets. Two different scenarios were studied: i) a reference case with the input parameters shown in Tables 4 and ii) an improved case with the better membrane properties shown in Table 5. The improved membranes properties were chosen as representative of properties better than those of the reference scenario, but are still realistic. For example, the electrical resistance of the membranes was reduced to 1/4th, so that the improved scenario is still characterized by values comparable with those exhibited by some commercial (Ran et al., 2017) and/or tailor-made membranes (Mei and Tang, 2018). Even lower values are possible, but they would be incompatible with the improvement of other properties, e.g. the selectivity (Luo et al., 2018).

Current density, mean channel flow velocity, inlet acid/base and salt concentrations were varied across a wide range of values.

4.2.1. Sensitivity on current density

The sensitivity analysis on the current density was performed with the mean flow velocity fixed at 1 cm s^{-1}, the inlet HCl and NaOH concentrations equal to 1 M (without salt), and the NaCl inlet concentration at 0.25 M. The current density was varied within the range of 50–200 A m^{-2}.

Fig. 6 shows the performance parameters as functions of the external current density for the two scenarios.

The GPD (Fig. 6a) increases significantly in the improved scenario due to the lower internal resistance. The GPD values range from a minimum of 5.6 W m^{-2} for the reference case, to a maximum of 38.1 W m^{-2} for the improved case. It is interesting to note that the reference case reaches the power peak at ~120 A m^{-2}, while the improved case is far from the power peak even at the highest current density considered in the simulations, i.e. 200 A m^{-2}. Therefore, the improved case may reach theoretically very high values of GPD, provided that BPMs are able to tolerate very high current densities without delamination issues. At the peak point of the reference case, the GPD is ~60% lower than the one reached at the same current density by the improved case.

The operating current density also affects the Gross Energy Density per unit mass of HCl (GED_m), which is reported in Fig. 6b. The improved and reference scenarios show maximum GED_m values around 100 and 80 A m^{-2}, respectively. Large differences were found in the GED_m values between the two scenarios of membrane properties over the whole range of simulated current densities. The improved GED_m was ~2.3 times higher than the reference GED_m.

Fig. 6c reports the HCl consumption as a function of the current density for the two scenarios, which exhibit no appreciable differences. For both scenarios, τ increases with the current density, as expected, ranging from ~7.6% to ~23%. The small decrease in HCl consumption in the improved case (6.4% in relative terms) is mainly due to the lower diffusive fluxes. The diffusive contribution to the HCl consumption, assessed by simulating perfect permselective membranes, was 2.9% and 1.5% on average for the reference and the improved scenario, respectively. The parasitic currents contribution to the HCl consumption, assessed by simulations without parasitic branches, was 0.6% and 1.1%

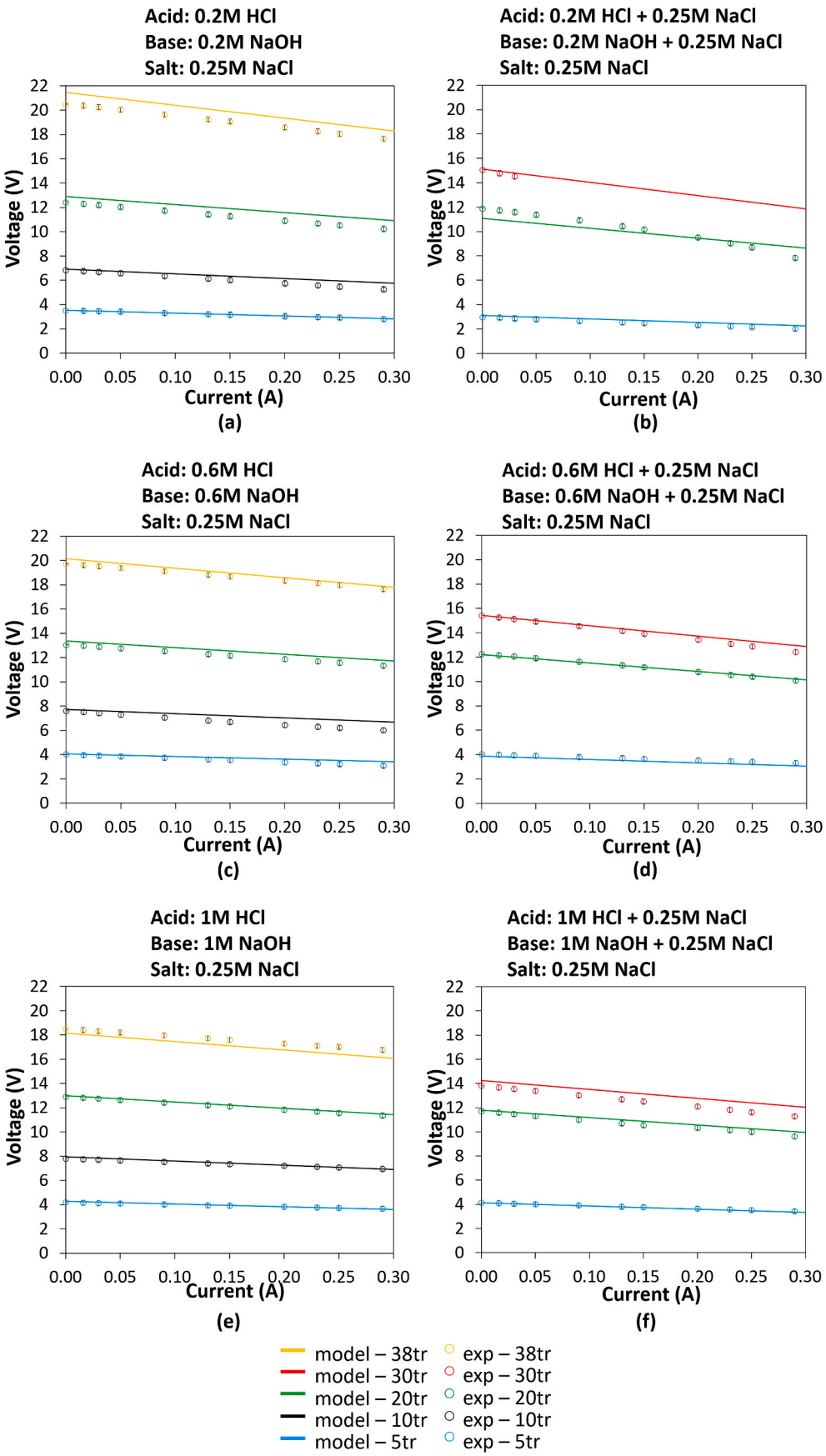

Fig. 4. Voltage-current curves by varying the number of triplets: comparison between model predictions (lines) and experimental results (points). Mean flow velocity of the electrolyte solutions in each channel equal to 1 cm s^{-1}. Areal blank resistance: 72 Ω cm^2.

Table 3
Summary of the inlet concentrations used for the experimental validation. Fluid velocity of 1 cm s^{-1} and current density of 29 A m^{-2}.

Test	N° triplets (–)	$C_{HCl,a,in}$ (mol m^{-3})	$C_{NaOH,b,in}$ (mol m^{-3})	$C_{NaCl,s,in}$ (mol m^{-3})
1	38	200	198	260
2	38	627	577	273
3	38	1032	998	284
4	30	212	193	268
5	30	622	671	276
6	30	1045	1165	287
7	20	199	183	245
8	20	600	555	257
9	20	1000	952	263

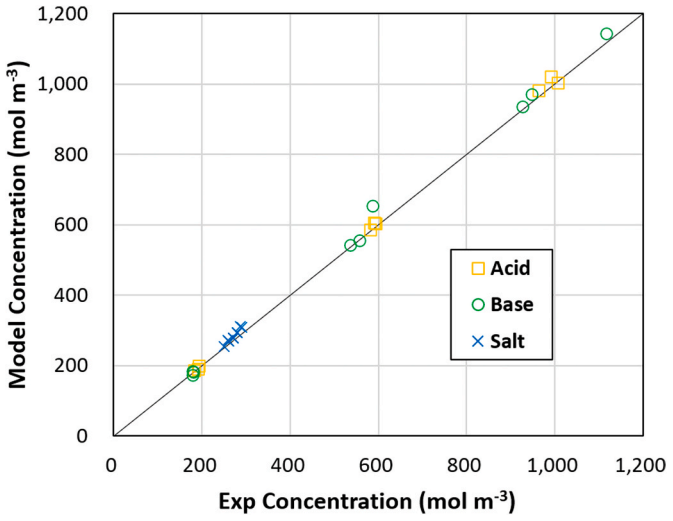

Fig. 5. Parity plots for the comparison of model outcome and experimental results for the concentration values at the stack outlet in BMRED tests with single-pass (fluid velocity of 1 cm s^{-1} and current density of 29 A m^{-2}): □ Outlet HCl concentration in the acid solution, ○ Outlet NaOH concentration in the base solution and × Outlet NaCl concentration in the salt solution.

Table 4
Inputs of the multi-scale model for the simulations of BMRED units. Membrane properties reported in Table 2 are maintained to simulate the reference scenario.

Geometrical features		
Spacer length	cm	50
Spacer width	cm	50
Spacer thickness	μm	500
Number of triplets	–	50
N° spacer holes	–	3
Spacer hole area	cm^2	1.7
Initial conditions of the solutions		
$C_{NaCl,a,in}$	mol m^{-3}	250
$C_{NaCl,b,in}$	mol m^{-3}	250
R_{bl}	Ω cm^2	72

Table 5
List of the membrane properties assumed for the improved scenario.

Improved membrane properties	
Electrical resistance	Current value (Table 2)/4
Ion diffusivities	Current value (Table 2)/2
Water permeability	Current value (Table 2)/2

on average for the reference and the improved scenario, respectively. In the improved scenario, although the membranes have better properties, there is an increase in the average cell current, which can be attributed to the non-linear trend of the parasitic currents as a function of the internal resistance. Moreover, it is worth noting that the outlet solutions have high acid and base content. Therefore, in the once-through mode, and with the investigated operating conditions, the energy extracted from the pH gradient is still low.

Finally, Fig. 6d illustrates the current efficiency as a function of the current density for the two scenarios with different membrane features. As expected, the current efficiency is higher in the improved scenario, as a result of the lower ion diffusion, and increases as the current density increases. From 50 to 200 A m^{-2}, the current efficiency increases by ~50% for both scenarios. Similarly to the current efficiency, the gross energy density was found to be higher in the improved scenario (Fig. 6b). This is due to the increase in the external voltage in the improved case, which also leads to higher GPD values (Fig. 6a).

4.2.2. Sensitivity on mean channel flow velocity

The effect of the mean flow velocity was analysed by fixing the current density at 100 A m^{-2}, the inlet HCl and NaOH concentrations equal to 1 M in the acid and base channels, respectively, and the NaCl inlet concentration in the salt channel at 0.25 M. The mean flow velocity was varied within the interval 0.5–5 cm s^{-1}.

Fig. 7a reports the Gross and Net power densities when varying the mean channel flow velocity for the reference and the improved scenarios.

No important differences in GPD were shown when varying the mean flow velocity for both the reference and improved scenarios. The average GPDs were 14.9 and 23.5 W m^{-2} for the reference and improved scenarios, respectively. The small increase in GPD at higher velocities is due to the higher average electromotive force. Instead, significant differences can be observed for the NPDs. Particularly, by increasing the mean flow velocity from 0.5 to 5 cm s^{-1}, NPD decreased by ~67% and ~42% for the reference and improved cases, respectively, reaching the maxima at a flow velocity of ~1 cm s^{-1}, and being very close to the GPD values at 0.5 cm s^{-1}. The different relative effect of the mean flow velocity on the NPD in the two scenarios is caused by the fact that the Pumping Power Density (function of the mean flow velocity) was practically the same.

No appreciable effects of the fluid velocity on the GED_m were observed. The average values were 0.27 and 0.49 kWh kg^{-1} for the reference and the improved scenarios, respectively.

Fig. 7b shows the HCl consumption as a function of the mean channel flow velocity for the reference and improved scenarios. The higher the mean flow velocity, the lower the HCl consumption, as expected. Particularly, from 0.5 cm s^{-1} to 5 cm s^{-1}, the HCl consumption was ~1 order of magnitude lower. Between the two scenarios, only a slight difference was found (i.e., an average relative difference of 8.1%), which is higher at low fluid velocity due to more important effects of diffusion.

The current efficiencies were found to be practically constant when varying the mean flow velocity. Specifically, the current efficiencies were 73 and 79% for the reference and improved case, respectively.

4.2.3. Sensitivity on inlet acid/base concentrations

The effect of the inlet acid/base concentration was assessed by fixing the current density at 100 A m^{-2}, the mean channel flow velocity at 1 cm s^{-1}, and the NaCl inlet concentration at 0.25 M. The inlet acid/base concentrations were varied within the range 0.2–1 M.

Fig. 8a shows the GPD by varying the acid/base inlet concentrations for the reference and improved scenarios.

The GPD shows an increasing trend towards a maximum, ranging from 6.57 to 14.7 W m^{-2} and from 14.8 to 23.4 W m^{-2} for the reference and improved scenarios, respectively. The increasing values can be simply explained by the higher electromotive force when raising the acid/base concentration. When applying the Nernst equation, the

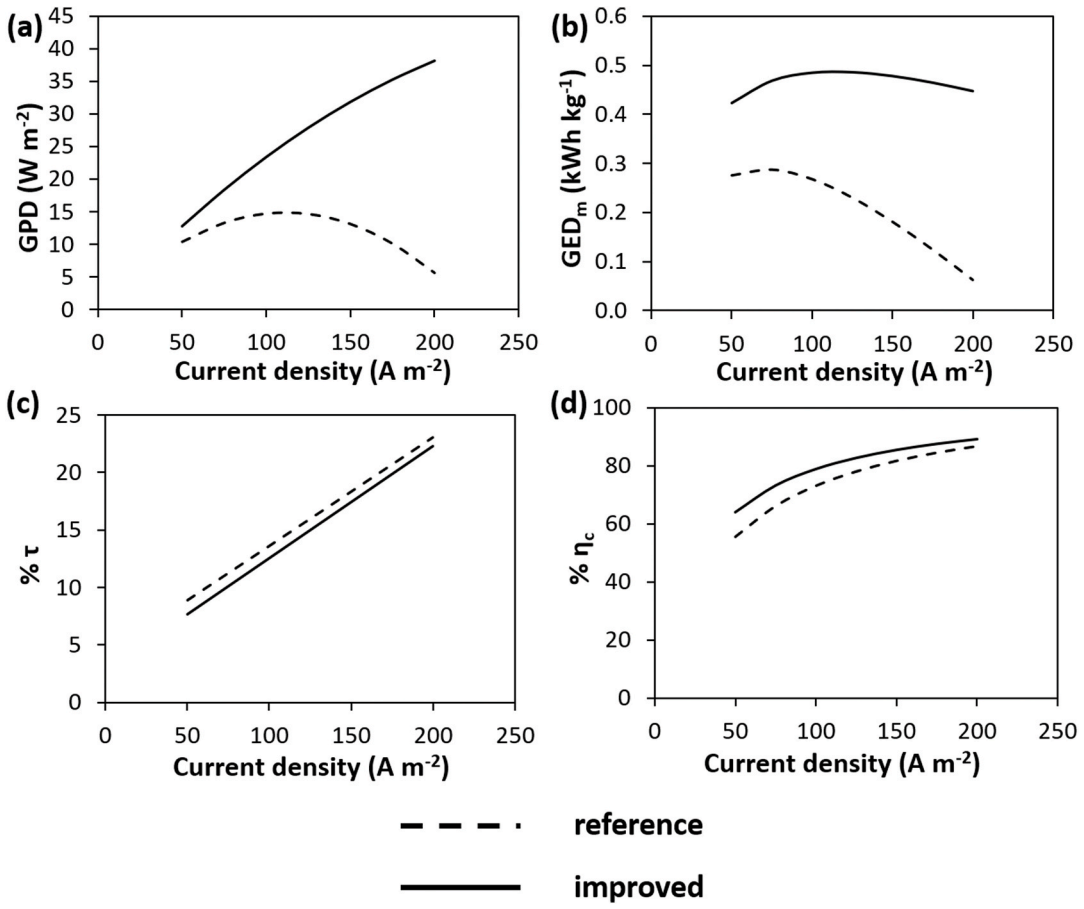

Fig. 6. (a) Gross Power Density (GPD), (b) Gross Energy Density per unit mass of HCl (GED_m), (c) HCl consumption (τ) and (d) Current efficiency (η_c) as functions of the current density for the reference and improved scenarios with a fixed mean flow velocity of 1 cm s^{-1}, inlet acid/base concentration 1 M and inlet salt concentration 0.25 M.

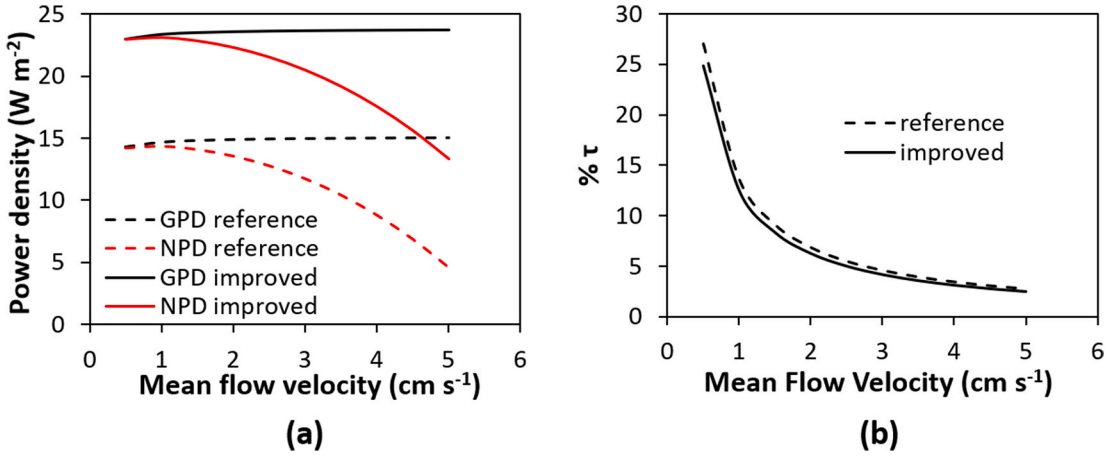

Fig. 7. (a) Gross Power Density (GPD) (black lines) and Net Power Density (NPD) (red lines) and (b) HCl consumption (τ) as functions of the mean flow velocity for the reference and improved scenarios with a fixed current density of 100 A m^{-2}, inlet acid/base concentration of 1 M and inlet salt concentration of 0.25 M. (For interpretation of the references to colour in this figure legend, the reader is referred to the Web version of this article.)

electromotive force in fact increases as the acid/base concentration increases, moving from 35.5 V to 42.1 V, i.e., 0.71 V and 0.84 V per triplet, respectively. The average relative difference of 41.5% in the GPD between the reference and the improved scenarios is a direct consequence of the reduced membranes resistance and, at a lesser extent, of the reduced diffusion.

Fig. 8b illustrates the results obtained for the Gross Energy Density per unit mass of HCl by varying the inlet acid/base concentration for the reference and improved scenarios. The results show that the GED_m curves exhibit increasing values that tend to flatten in the upper range of acid/base concentrations. Overall, from 0.2 M to 1 M of acid/base, the GED_m varies by 54 and 22% for the reference and the improved case, respectively.

Fig. 8c shows the HCl consumption curve as a function of the inlet

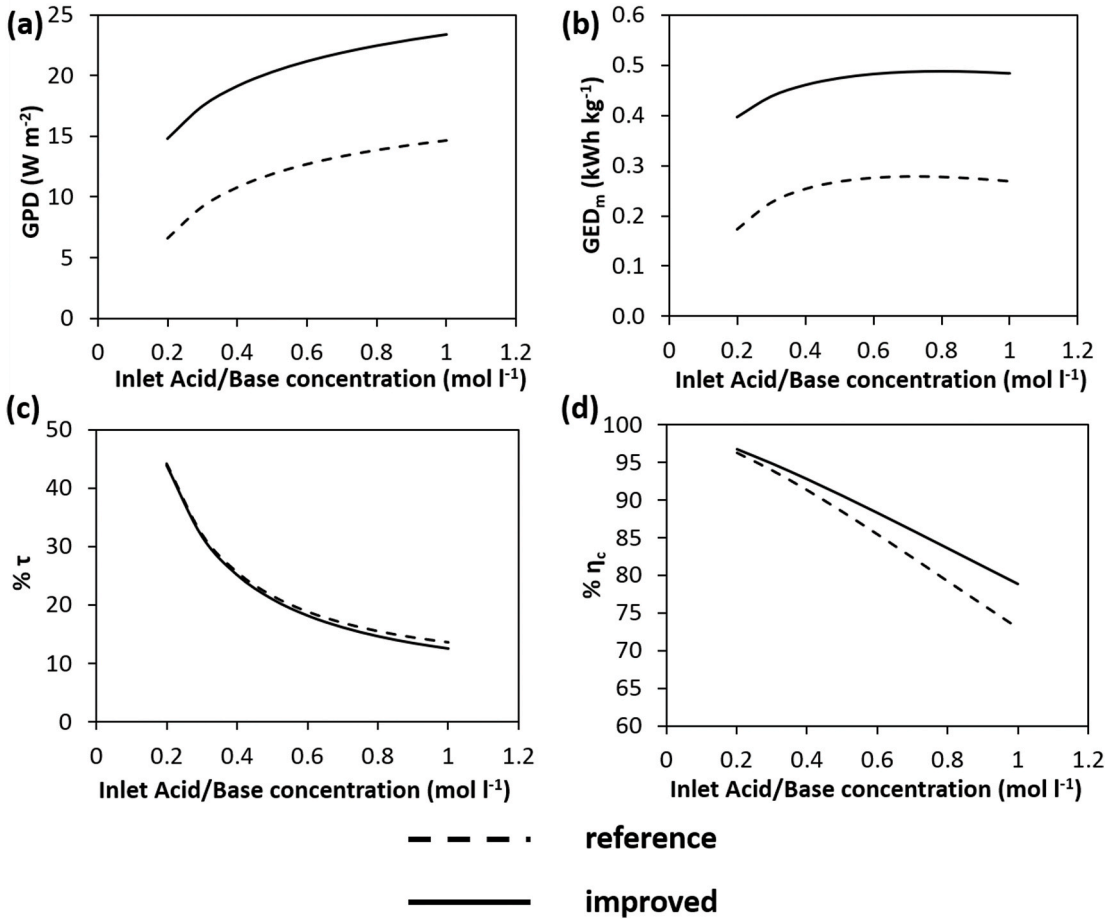

Fig. 8. (a) Gross Power Density (GPD), (b) Gross Energy Density per unit mass (GED_m), (c) HCl consumption (τ) and (d) Current efficiency (η_c) as a function of the inlet acid/base concentration for the reference and improved scenarios with a fixed current density of 100 A m^{-2}, a mean flow velocity of 1 cm s^{-1} and an inlet salt concentration of 0.25 M.

acid/base concentration for the investigated scenarios. HCl consumption values differ by ~3% on average in the two different scenarios. The pronounced decreasing trend is a consequence of the inverse relationship between HCl consumption and inlet acid concentration. The ion diffusion could soften this behaviour; however, the small differences between the two scenarios indicate small effects of ion diffusion. Fig. 8d illustrates the current efficiency as a function of the inlet acid/base concentration for the two scenarios. By increasing the acid/base concentration within the investigated range, the current efficiency decreases, losing 23.2 and 17.9 percentage points for the reference and improved cases, respectively. This behaviour is due to larger diffusion and parasitic currents at higher inlet acid/base concentrations. Particularly, by increasing the inlet acid/base concentrations, the resulting cell currents increase, leading to higher values of inlet-outlet concentration differences and, thus, to lower values of current efficiency. Moreover, the reduction of the current efficiency explains the decreasing rate of increase of energy density per unit mass of transported acid shown in Fig. 8b.

4.2.4. Sensitivity on inlet salt concentration

The effect of the inlet salt concentration was evaluated by fixing the current density at 100 A m^{-2}, the mean channel flow velocity at 1 cm s^{-1}, and the HCl and NaOH inlet concentrations at 1 M. The inlet salt concentration was varied within the range 0.001–1 M.

Fig. 9a shows the GPD by varying the salt inlet concentration in the reference and improved scenarios.

GPD shows a slight decreasing trend as the salt concentration increases, ranging from 15.3 to 13.4 W m^{-2} for the reference case and from 23.9 to 22.1 W m^{-2} for the improved case. Similarly, the GED_m values decrease (Fig. 9b) with relative variations of 7.3 and 5.5% in the reference and improved case, respectively. Compared to the reference case, the improved case exhibited lower values of HCl consumption (Fig. 9c). Particularly, HCl consumption values differ by ~1% on average in the two different scenarios. Finally, no important variations were recorded in the current efficiency when varying the salt inlet concentrations (Fig. 9d). The averaged values were 72.9% and 78.9% for the reference and improved scenarios, respectively.

4.3. Example of an industrial BMRED scheme for energy recovery from waste streams

In this section, a possible scheme for industrial application of energy recovery via BMRED from waste streams is designed.

The stack size is the same as the one reported in section 4.2. It is worth noting that, depending on the capacity of the industrial plant, the number of BMRED modules must be increased to meet the requirement in terms of flow rates of processed wastes. For example, configurations with several units hydraulically in parallel could be beneficial for this purpose.

The neutralization of waste acid and base solutions from the pickling and the manufacturing industries was considered. HCl and NaOH waste solutions were simulated with the presence of background salt. It is well known that exhausted solutions from pickling operations range from 20 to 150 g l^{-1} (Gueccia et al., 2020). Spent caustic soda solutions may present a concentration of around 4% weight (Rahman and Khan, 2010). The present simulations assessed the energetic yield of a multi-stage

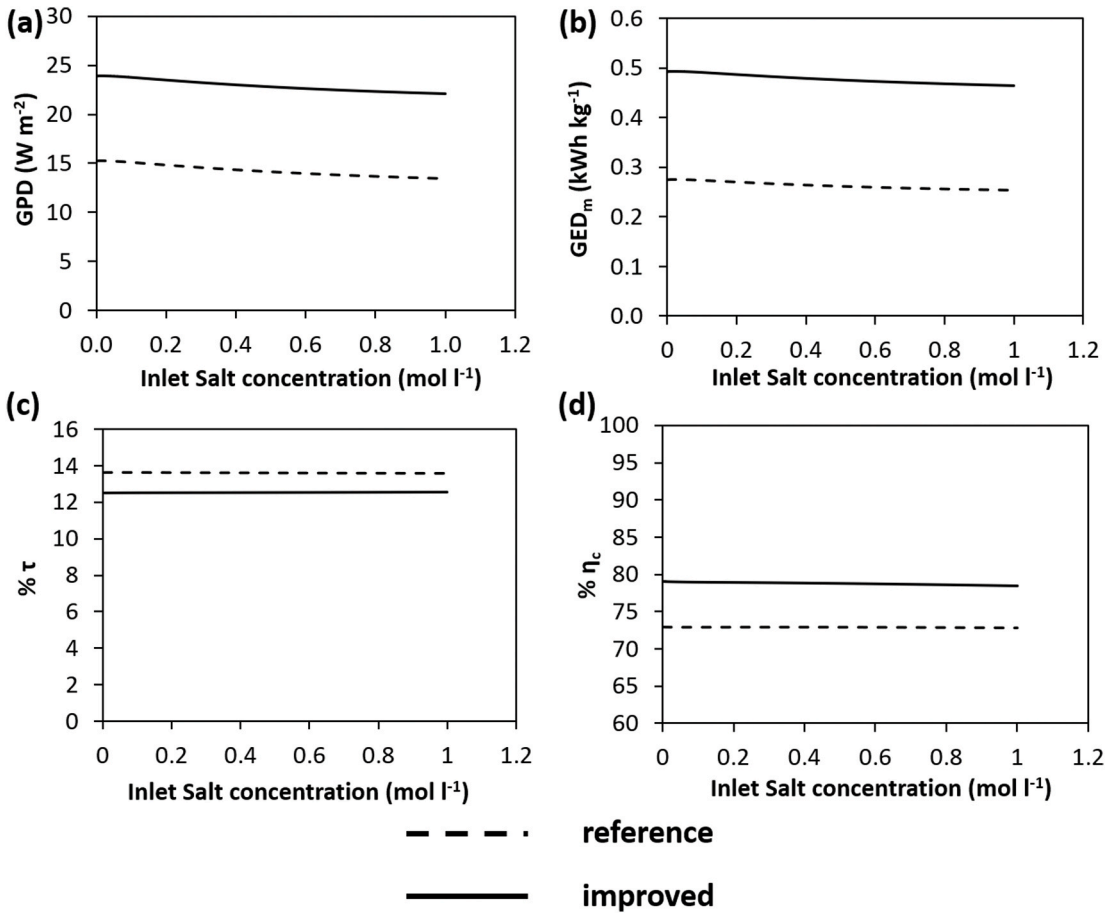

Fig. 9. (a) Gross Power Density (GPD), (b) Gross Energy Density per unit mass (GED_m), (c) HCl consumption (τ) and (d) Current efficiency (η_c) as a function of the inlet salt concentration for the reference and improved scenarios with a fixed current density of 100 A m^{-2}, a mean flow velocity of 1 cm s^{-1} and inlet acid/base concentrations of 1 M.

process. Energy density and process efficiency were evaluated following the approach formulated in section 2.4, with the stack features shown for the improved scenario in section 4.2 (Tables 4 and 5). Instead, the acid, base and salt solution composition and concentrations are reported in Table 6.

Since the acid and base concentrations are different, a possible process scheme to reduce their concentration at the same value could be a multi-stage system with the acid solution processed sequentially and the base and salt solutions processed singularly (Fig. 10). In this way, the outlet concentration of both the acidic solution (from the last stage) and the alkaline solution (from each stage) was close to zero, thus obtaining a high degree of neutralization for both solutions.

Simulation results showed that 15 BMRED stages were needed for the complete neutralization of the acid solution. The gross energy density was 53.5 and 48.3 kWh m^{-3} of acidic solution in the two cases of 1 M and 0.3 M of inlet concentration of NaOH, respectively. Interestingly, even using a spent sodium hydroxide solution of less than 1.2% weight

Table 6
Initial composition and concentrations used to simulate a possible industrial BMRED scheme.

Inlet composition and concentrations		
$C_{HCl,a,in}$	mol m^{-3}	2700
$C_{NaCl,a,in}$	mol m^{-3}	250
$C_{NaCl,s,in}$	mol m^{-3}	250
$C_{NaOH,b,in}$	mol m^{-3}	300 or 1000
$C_{NaCl,b,in}$	mol m^{-3}	250

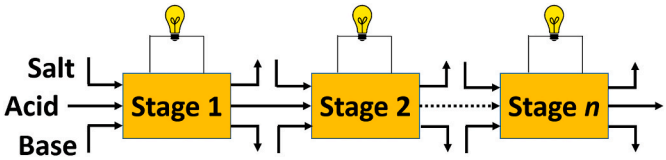

Fig. 10. Scheme of the multi-stage BMRED process.

(i.e., ~0.3 M), the energy efficiency was 82%, while by using 1 M of inlet NaOH concentration it reached 91%. Under equal current density, the use of a more concentrated base solution (i.e., 1 M NaOH) causes an increase in the average power per stage. This fact leads to a higher GED_v resulting in a higher energy efficiency.

These interesting preliminary results suggest that neutralizing waste acid/base streams in BMRED units to produce electric power may be a very promising option which should be further investigated to eventually lead its technology development up to the implementation in real industrial sites.

5. Conclusions

BMRED represents a promising system to harvest energy from the neutralization of acid and base streams. In this work, a process model developed in our previous work (Culcasi et al., 2020b) was improved by including a more realistic simulation of the bipolar membrane. The present BMRED process model was validated against single-pass experiments, showing a good agreement under several operating

conditions. This reliable and flexible modelling tool was then used to perform a sensitivity analysis of the BMRED performance to several process parameters (external current density, flow velocity inside the channels, acid and base inlet concentrations and salt inlet concentration).

The results were promising, showing that net power densities of ~15 W m^{-2} are achievable with current commercial membranes. High-performance membranes would increase the net power density up to ~25 W m^{-2} or even significantly higher values, provided that BPMs could tolerate high current densities without damage due to delamination. Moreover, the simulation of an industrial scheme predicted an energy density of ~50 kWh m^{-3} (of acid solution) with energy efficiency of ~80–90% for the neutralization of acid and alkaline solutions by using improved membranes, thus showing the huge potential of BMRED systems for energy harvesting by use of waste streams. Membranes play a key role; therefore, the development of high-performance membranes is crucial for the process competitiveness. Improvements in the process performance can be expected also by optimising operating conditions and stack design. Further studies should address these aspects, the techno-economic assessment, the use of real industrial wastewater and the conceptual design of complete treatment lines.

Author statement

Andrea Culcasi, Methodology, Software, Formal analysis, Investigation, Writing – original draft, Visualization. Luigi Gurreri, Conceptualization, Methodology, Validation, Formal analysis, Data curation, Writing – review & editing, Supervision. Giorgio Micale, Conceptualization, Methodology, Resources, Writing – review & editing, Supervision, Project administration, Funding acquisition. Alessandro Tamburini, Conceptualization, Methodology, Validation, Resources, Writing – review & editing, Supervision, Project administration, Funding acquisition.

Declaration of competing interest

The authors declare that they have no known competing financial interests or personal relationships that could have appeared to influence the work reported in this paper.

Acknowledgments

This work was performed in the framework of the BAoBaB project (*Blue Acid/Base Battery: Storage and recovery of renewable electrical energy by reversible salt water dissociation*). The BAoBaB project has received funding from the European Union's Horizon 2020 Research and Innovation program under Grant Agreement no. 731187 (www.baobabproject.eu). Dr. Andrea Zaffora and Mr. Alessandro Cosenza are greatly acknowledged for collecting the experimental data employed for model validation.

References

Agrawal, A., Sahu, K.K., 2009. An overview of the recovery of acid from spent acidic solutions from steel and electroplating industries. J. Hazard Mater. 171, 61–75. https://doi.org/10.1016/j.jhazmat.2009.06.099.

Battaglia, G., Gurreri, L., Ciofalo, M., Cipollina, A., Bogle, I.D.L., Pirrotta, A., Micale, G., 2021. A 2-D model of electrodialysis stacks including the effects of membrane deformation. Desalination 500, 114835. https://doi.org/10.1016/j.desal.2020.114835.

Campione, A., Cipollina, A., Toet, E., Gurreri, L., Bogle, I.D.L., Micale, G., 2020. Water desalination by capacitive electrodialysis: experiments and modelling. Desalination 473, 114150. https://doi.org/10.1016/J.DESAL.2019.114150.

Ciofalo, M., La Cerva, M., Di Liberto, M., Gurreri, L., Cipollina, A., Micale, G., 2019. Optimization of net power density in Reverse Electrodialysis. Energy 181, 576–588. https://doi.org/10.1016/j.energy.2019.05.183.

Culcasi, A., Gueccia, R., Randazzo, S., Cipollina, A., Micale, G., 2019. Design of a novel membrane-integrated waste acid recovery process from pickling solution. J. Clean. Prod. 236, 117623. https://doi.org/10.1016/j.jclepro.2019.117623.

Culcasi, A., Gurreri, L., Zaffora, A., Cosenza, A., Tamburini, A., Cipollina, A., Micale, G., 2020a. Ionic shortcut currents via manifolds in reverse electrodialysis stacks. Desalination 485, 114450. https://doi.org/10.1016/j.desal.2020.114450.

Culcasi, A., Gurreri, L., Zaffora, A., Cosenza, A., Tamburini, A., Micale, G., 2020b. On the modelling of an Acid/Base Flow Battery: an innovative electrical energy storage device based on pH and salinity gradients. Appl. Energy 277, 115576. https://doi.org/10.1016/j.apenergy.2020.115576.

Emrén, A.T., Holmström, V.J.M., 1983. Energy storage in a fuel cell with bipolar membranes burning acid and hydroxide. Energy 8, 277–282. https://doi.org/10.1016/0360-5442(83)90103-2.

Generous, M.M., Qasem, N.A.A., Zubair, S.M., 2020. The significance of modeling electrodialysis desalination using multi-component saline water. Desalination 496, 114347. https://doi.org/10.1016/j.desal.2020.114347.

Goel, R.K., Flora, J.R.V., Chen, J.P., 2005. Flow equalization and neutralization. In: Wang, L.K., Hung, Y.-T., Shammas, N.K. (Eds.), Physicochemical Treatment Processes. Humana Press, Totowa, NJ, NJ, pp. 21–45. https://doi.org/10.1385/1-59259-820-x:021.

Gueccia, R., Aguirre, A.R., Randazzo, S., Cipollina, A., Micale, G., 2020. Diffusion dialysis for separation of hydrochloric acid, iron and zinc ions from highly concentrated pickling solutions. Membranes 10, 129. https://doi.org/10.3390/membranes10060129.

Gurreri, L., Tamburini, A., Cipollina, A., Micale, G., 2020. Electrodialysis applications in wastewater treatment for environmental protection and Resources recovery: a systematic review on progress and perspectives. Membranes 10, 146. https://doi.org/10.3390/membranes10070146.

Imran, B., Khan, S.J., Qazi, I.A., Arshad, M., 2016. Removal and recovery of sodium hydroxide (NaOH) from industrial wastewater by two-stage diffusion dialysis (DD) and electrodialysis (ED) processes. Desalin. Water Treat. 57, 7926–7932. https://doi.org/10.1080/19443994.2015.1048742.

Kim, J.H., Lee, J.H., Maurya, S., Shin, S.H., Lee, J.Y., Chang, I.S., Moon, S.H., 2016. Proof-of-concept experiments of an acid-base junction flow battery by reverse bipolar electrodialysis for an energy conversion system. Electrochem. Commun. 72, 157–161. https://doi.org/10.1016/j.elecom.2016.09.025.

Kontturi, K., Murtomäki, L., Manzanares, J.A., 2008. Ionic Transport Processes, Ionic Transport Processes: in Electrochemistry and Membrane Science. Oxford University Press. https://doi.org/10.1093/acprof:oso/9780199533817.001.0001.

Kraaijeveld, G., Sumberova, V., Kuindersma, S., Wesselingh, H., 1995. Modelling electrodialysis using the Maxwell-Stefan description. Chem. Eng. J. Biochem. Eng. J. 57, 163–176. https://doi.org/10.1016/0923-0467(94)02940-7.

La Cerva, M., Gurreri, L., Cipollina, A., Tamburini, A., Ciofalo, M., Micale, G., 2019. Modelling and cost analysis of hybrid systems for seawater desalination: electromembrane pre-treatments for Reverse Osmosis. Desalination 467, 175–195. https://doi.org/10.1016/j.desal.2019.06.010.

Luo, T., Abdu, S., Wessling, M., 2018. Selectivity of ion exchange membranes: a review. J. Membr. Sci. 555, 429–454. https://doi.org/10.1016/j.memsci.2018.03.051.

Mei, Y., Tang, C.Y., 2018. Recent developments and future perspectives of reverse electrodialysis technology: a review. Desalination 425, 156–174. https://doi.org/10.1016/j.desal.2017.10.021.

Pärnamäe, R., Gurreri, L., Post, J., van Egmond, W.J., Culcasi, A., Saakes, M., Cen, J., Goosen, E., Tamburini, A., Vermaas, D.A., Tedesco, M., 2020. The acid–base flow battery: sustainable energy storage via reversible water dissociation with bipolar membranes. Membranes 10, 409. https://doi.org/10.3390/membranes10120409.

Pärnamäe, R., Mareev, S., Nikonenko, V., Melnikov, S., Sheldeshov, N., Zabolotskii, V., Hamelers, H.V.M., Tedesco, M., 2021. Bipolar membranes: a review on principles, latest developments, and applications. J. Membr. Sci. 617, 118538. https://doi.org/10.1016/j.memsci.2020.118538.

Pretz, J., Staude, E., 1998. Reverse electrodialysis (RED) with bipolar membranes, an energy storage system. Berichte der Bunsengesellschaft für Phys. Chemie 102, 676–685. https://doi.org/10.1002/bbpc.19981020412.

Rahman, M.A., Khan, N.E., 2010. Study of an evaporation system for sodium hydroxide solution. J. Chem. Eng. 24, 35–36. https://doi.org/10.3329/jce.v24i0.5581.

Ramírez, P., Rapp, H.J., Mafé, S., Bauer, B., 1994. Bipolar membranes under forward and reverse bias conditions. Theory vs. experiment. J. Electroanal. Chem. 375, 101–108. https://doi.org/10.1016/0022-0728(94)03379-X.

Ran, J., Wu, L., He, Y., Yang, Z., Wang, Y., Jiang, C., Ge, L., Bakangura, E., Xu, T., 2017. Ion exchange membranes: new developments and applications. J. Membr. Sci. 522, 267–291. https://doi.org/10.1016/j.memsci.2016.09.033.

Tanaka, Y., 2007. Ion Exchange Membranes: Fundamentals and Applications, Membrane Science and Technology. Elsevier, Amsterdam. https://doi.org/10.1016/S0927-5193(07)12021-0.

Tansens, P., Rodal, A.T., Machado, C.M.M., Soares, H.M.V.M., 2011. Recycling of aluminum and caustic soda solution from waste effluents generated during the cleaning of the extruder matrixes of the aluminum industry. J. Hazard Mater. 187, 459–465. https://doi.org/10.1016/j.jhazmat.2011.01.048.

Tedesco, M., Hamelers, H.V.M., Biesheuvel, P.M., 2017. Nernst-Planck transport theory for (reverse) electrodialysis: II. Effect of water transport through ion-exchange membranes. J. Membr. Sci. 531, 172–182. https://doi.org/10.1016/j.memsci.2017.02.031.

van Egmond, W.J., Saakes, M., Noor, I., Porada, S., Buisman, C.J.N., Hamelers, H.V.M., 2018. Performance of an environmentally benign acid base flow battery at high energy density. Int. J. Energy Res. 42, 1524–1535. https://doi.org/10.1002/er.3941.

Veerman, J., Saakes, M., Metz, S.J., Harmsen, G.J., 2010. Reverse electrodialysis: evaluation of suitable electrode systems. J. Appl. Electrochem. 40, 1461–1474. https://doi.org/10.1007/s10800-010-0124-8.

Walther, James F., Skaneateles, N.Y., 1982. Process for Production of Electrical Energy from the Neutralization of Acid and Base in a Bipolar Membrane Cell. US4311771A.

Xia, J., Eigenberger, G., Strathmann, H., Nieken, U., 2020. Acid-base flow battery, based on reverse electrodialysis with bi-polar membranes: stack experiments. Processes 8, 99. https://doi.org/10.3390/pr8010099.

Xia, J., Eigenberger, G., Strathmann, H., Nieken, U., 2018. Flow battery based on reverse electrodialysis with bipolar membranes: single cell experiments. J. Membr. Sci. 565, 157–168. https://doi.org/10.1016/j.memsci.2018.07.073.

Zaffora, A., Culcasi, A., Gurreri, L., Cosenza, A., Tamburini, A., Santamaria, M., Micale, G., 2020. Energy harvesting by waste acid/base neutralization via bipolar membrane reverse electrodialysis. Energies 13, 5510. https://doi.org/10.3390/en13205510.

Zholkovskij, E.K., Müller, M.C., Staude, E., 1998. The storage battery with bipolar membranes. J. Membr. Sci. 141, 231–243. https://doi.org/10.1016/S0376-7388(97)00306-2.